

Numerical investigation of effect of crack geometrical parameters on hydraulic fracturing process of hydrocarbon reservoirs

A. Abdollahipour*, M. Fatehi Marji, A.R. Yarahmadi Bafghi and J. Gholamnejad

Department of Mining and Metallurgical Engineering, Yazd University, Yazd, Iran

Received 7 October 2015; received in revised form 22 November 2015; accepted 24 November 2015

*Corresponding author: ab.abdollahipour@gmail.com (A. Abdollahipour).

Abstract

Hydraulic fracturing (HF), as a stimulation technique in petroleum engineering, has made possible the oil production from reservoirs with very low permeability. The combination of horizontal drilling and multiple HF with various perforation angles has been widely used to stimulate oil reservoirs for economical productions. Despite the wide use of HF, there are still ambiguous aspects that require more investigation. Therefore, optimizing the geometry of the initial fractures using numerical methods is of high importance in a successful HF operation. Different geometrical parameters of the initial HF cracks including patterns, spacings, crack lengths, and perforation phase angles were modeled using the higher order displacement discontinuity method (HODDM) in horizontal and vertical oil wells. Several well-known issues in HF such as crack interference and crack arrest were observed in certain patterns of the HF cracks. Also the best possible arrangements of the HF cracks were determined for a better production. The results obtained were verified by the in-situ measurements existing in the literature. In addition, the best perforation phase angle in vertical wells was investigated and determined.

Keywords: *Hydraulic Fracturing, Well Stimulation, Crack Propagation, Crack Interference, Perforation.*

1. Introduction

The combination of horizontal drilling and multiple hydraulic fracturing (HF) has been recognized as a successful stimulation technique for an enhanced hydrocarbon recovery from low permeability reservoirs. The primary objective of HF is to improve the natural connections of wellbores and reservoirs. Although it is a widespread method used in oil and gas exploitations, there are fundamental aspects that are yet ambiguous and require further investigations to eventually increase the HF efficiency. One of these aspects is the arrangement of the initial perforations in relation to each other and in relation to the in-situ stress regime. The orientation of a wellbore and prevailing the in-situ stress regime have important effects on the initiation of a HF process [1].

Multiple transverse hydraulic fractures in a horizontal wellbore can create a large stimulated reservoir volume (SRV), which is the main

contributor to a high hydrocarbon production [2–8]. Long laterals require a greater volume of liquids and proppants, contributing to a higher cost [9]. Therefore, optimization of the hydraulic fracture parameters such as the fracture spacing and fracture half-length is important.

It has been shown that an increase in the number of fractures in the formation around the wellbore results in a faster hydrocarbon production [10, 11]. In some cases, more than 20 fracture stages have been tried in a horizontal well in order to increase the fracture contact with the formation, and to produce high initial rates. The studies have suggested that the initial production increases linearly with the number of fractures but a high flow rate is not sustainable and declines sharply once the fractures interfere over a given lateral length [12, 13]. It is obvious that the longer the initial fracture length and the shorter their spacings, the higher the oil production will be.

However, reduction in the fracture spacing is expensive, and may even cause interference and subsequent reduction in the hydrocarbon production [14–16], which could be a cause of near-wellbore tortuosity or even pinching, a factor that usually determines the success or failure of the HF treatments [17–19].

Development of the near-wellbore fracture complexity, with associated pinching and competition between multiple fracture branches, can occur simultaneously in the evolution of fracture paths. The numerical HF models have been applied to the study of problems dealing with competing fracture propagation, conditions of fracture initiation, and propagation and interaction of multiple fractures [20–25]. In this paper, a 2D higher order displacement discontinuity method (HODDM) was employed to study the behavior of multi-stage fractures with different spacings and pre-existing or perforated fracture (PF) half-lengths. Also the effect of orientation on the fracture development was studied.

2. Geometrical and mechanical properties of initial model

Rock mass was assumed to be impermeable, and a uniform pressure was considered in PFs. The following properties (based on the field data [26]) and assumptions were also considered through the analysis, unless stated otherwise:

- The wellbore axis is aligned with one of the principal horizontal stresses, and has the radius $R = 0.1 \text{ m}$.
- $\sigma_v = 64 \text{ MPa}$ and $\sigma_h = 47 \text{ MPa}$ are the far-field principal stresses.
- The internal pressure in PFs and wellbore is $P = 30 \text{ MPa}$.
- The geomechanical properties are considered in the analyses including modulus of elasticity $E = 40 \text{ GPa}$, Poisson ratio $\nu = 0.2$, and fracture toughness $K_{IC} = 3 \text{ MPa}\sqrt{\text{m}}$.
- The model is in a depth of 2500 m, and the compressive and tensile strengths of the host rock are, respectively, 110 and 17.5 MPa.
- The maximum tangential stress mixed mode fracture criterion, proposed by Erdogan and Sih [27], is used to determine the crack initiation angle θ based on the linear elastic fracture mechanics principles [28–31].

To generalize the results obtained, the normalized parameter $\beta = S/L$ was proposed and used through the analyses, where $S \text{ (m)}$ is the spacing, and $L \text{ (m)}$ is the fracture length.

3. HODDM

A 2D code based on the displacement discontinuity method was used to investigate the initiation and propagation of the fractures from a wellbore. Cubic element displacement discontinuity, which is based on the analytical integration of the cubic collocation shape functions over collinear or straight-line displacement discontinuity elements [32], was added to achieve a higher accuracy. Due to the singularity variations, the accuracy of the displacement discontinuity method at the vicinity of the crack tips decreases, and therefore, a special crack tip element was also considered at the tip of each crack to increase the accuracy efficiency of the method. The far field in-situ stresses were changed to the local normal and shear stresses on each element using appropriate stress transition equations. Then the resulting normal or shear local stresses were summed up under the appropriate boundary conditions (if there was any stress boundary) to produce the actual stress state on each element [33].

3.1. Cubic element formulation

Much higher accuracies of the displacement discontinuities along the boundary of the problem can be achieved using the higher order displacement discontinuity (*DD*) elements (e.g. quadratic or cubic *DD* elements) in the solution of elastostatic cracked bodies.

A cubic *DD* element ($D_k(\eta)$) is divided into four equal sub-elements, and each sub-element contains a central node, for which the nodal *DD* is evaluated numerically (the opening displacement discontinuity D_y and sliding displacement discontinuity D_x) [34].

$$D_k(\eta) = \sum_{i=1}^4 N_i(\eta) D_k^i, \quad k = x, y \quad (1)$$

where D_k^i (i.e. D_x^i and D_y^i) with ($i = 1$ to 4) are the cubic nodal displacement discontinuities, and

$$\begin{aligned} N_1(\eta) &= -(3a_1^3 - a_1^2\eta - 3a_1\eta^2 + \eta^3)/(48a_1^3), \\ N_2(\eta) &= (9a_1^3 - 9a_1^2\eta - a_1\eta^2 - \eta^3)/(16a_1^3), \\ N_3(\eta) &= (9a_1^3 + 9a_1^2\eta - a_1\eta^2 - \eta^3)/(16a_1^3), \\ N_4(\eta) &= -(3a_1^3 + a_1^2\eta - 3a_1\eta^2 - \eta^3)/(48a_1^3) \end{aligned} \quad (2)$$

are the cubic collocation shape functions using $a_1 = a_2 = a_3 = a_4$. A cubic element is shown in Figure 1 (a).

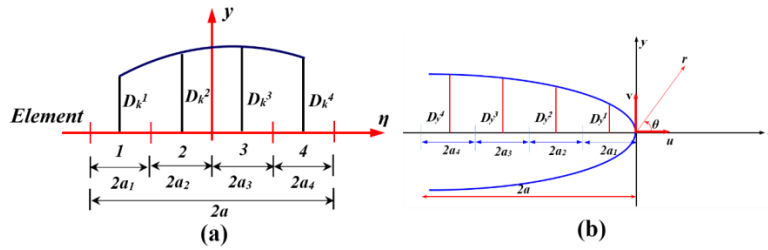


Figure 1. a) Cubic collocation for cubic element displacement discontinuity, and b) displacement correlation technique for special crack tip element [35].

The displacements and stresses for a line crack in an infinite body along the *x*-axis, in terms of the single harmonic functions *g(x,y)* and *f(x,y)*, are [36]:

$$\begin{aligned} u_x &= [2(1-\nu)f_{,y} - yf_{,xx}] + [-(1-2\nu)g_{,x} - yg_{,xy}] \\ u_y &= [(1-2\nu)f_{,x} - yf_{,xy}] + [2(1-\nu)g_{,y} - yg_{,yy}] \end{aligned} \quad (3)$$

and the stresses are:

$$\begin{aligned} \sigma_{xx} &= 2\mu[2f_{,xy} + yf_{,xyy}] + 2\mu[g_{,yy} + yg_{,yyy}] \\ \sigma_{yy} &= 2\mu[-yf_{,xyy}] + 2\mu[g_{,yy} - yg_{,yyy}] \\ \sigma_{xy} &= 2\mu[2f_{,yy} + yf_{,yyy}] + 2\mu[-yg_{,xyy}] \end{aligned} \quad (4)$$

μ is the shear modulus, and $f_{,x}$, $g_{,x}$, $f_{,y}$, $g_{,y}$, etc. are the partial derivatives of the single harmonic functions *f(x,y)* and *g(x,y)* with respect to *x* and *y*, in which these potential functions for the cubic element case can be found from:

$$\begin{aligned} f(x,y) &= \frac{-1}{4\pi(1-\nu)} \sum_{j=1}^4 D_x^j F_j(I_0, I_1, I_2, I_3) \\ g(x,y) &= \frac{-1}{4\pi(1-\nu)} \sum_{j=1}^4 D_y^j F_j(I_0, I_1, I_2, I_3) \end{aligned} \quad (5)$$

in which the common function F_j is defined as:

$$F_j(I_0, I_1, I_2, I_3) = \int_{-a}^a N_j(\eta) \ln \sqrt{(x-\eta)^2 + y^2} d\eta, \quad (6)$$

j= 1, to 4

where I_0 to I_3 are the integrals distributed from $-a$ to $+a$. The integrals have been explained in details in [33, 35].

3.2. Special crack tip element

Since the singularities of the stresses and displacements near the crack ends may reduce their accuracies, the special crack tip elements are used to increase the accuracy of the *DDs* near the crack tips [35]. As shown in Figure 1 (b), the *DD* variation for four nodes can be formulated using a special crack tip element containing four nodes (or having four special crack tip sub-elements).

$$\begin{aligned} D_{c1}(\eta) &= [N_{c1}(\eta)]D_{c1}^1(a) + [N_{c2}(\eta)]D_{c1}^2(a) + \\ & [N_{c3}(\eta)]D_{c1}^3(a) + [N_{c4}(\eta)]D_{c1}^4(a) \end{aligned} \quad (7)$$

where the crack tip element has a length $a_1 = a_2 = a_3 = a_4$.

Considering a crack tip element with four equal sub-elements ($a_1 = a_2 = a_3 = a_4$), the shape functions $N_{C1}(\eta)$ to $N_{C4}(\eta)$ can be obtained as equations:

$$\begin{aligned} N_{C1}(\eta) &= 2.1336 \left(\frac{\eta}{a_1}\right)^2 - 1.3965 \left(\frac{\eta}{a_1}\right)^3 + 0.2759 \left(\frac{\eta}{a_1}\right)^5 - 0.0172 \left(\frac{\eta}{a_1}\right)^7 \\ N_{C2}(\eta) &= -0.9475 \left(\frac{\eta}{a_2}\right)^2 + 1.2094 \left(\frac{\eta}{a_2}\right)^3 - 0.2787 \left(\frac{\eta}{a_2}\right)^5 + 0.0194 \left(\frac{\eta}{a_2}\right)^7 \\ N_{C3}(\eta) &= 0.1908 \left(\frac{\eta}{a_3}\right)^2 - 0.2467 \left(\frac{\eta}{a_3}\right)^3 + 0.0771 \left(\frac{\eta}{a_3}\right)^5 - 0.0231 \left(\frac{\eta}{a_3}\right)^7 \\ N_{C4}(\eta) &= -0.0977 \left(\frac{\eta}{a_4}\right)^2 + 0.150 \left(\frac{\eta}{a_4}\right)^3 - 0.0586 \left(\frac{\eta}{a_4}\right)^5 + 0.0065 \left(\frac{\eta}{a_4}\right)^7 \end{aligned} \quad (8)$$

By substituting Eqs. (8) into Eqs. (7) and then substituting these equations into Eqs. (3) and (4), and following the procedures similar to those given for the derivation of the general potential function $F_j(I_0, I_1, I_2, I_3)$ in Eq. (6), the general potential function $F_C(x,y)$ for the crack tip element can be expressed as:

$$\begin{aligned} F_C(x,y) &= -\frac{1}{4\pi(1-\nu)} \left\{ \left[\int_{-a}^a N_{C1}(\eta) \ln \left[(x-\eta)^2 + y^2 \right]^{0.5} d\eta D_1^1 \right] + \right. \\ & \left[\int_{-a}^a N_{C2}(\eta) \ln \left[(x-\eta)^2 + y^2 \right]^{0.5} d\eta D_1^2 \right] + \\ & \left[\int_{-a}^a N_{C3}(\eta) \ln \left[(x-\eta)^2 + y^2 \right]^{0.5} d\eta D_1^3 \right] + \\ & \left. \left[\int_{-a}^a N_{C4}(\eta) \ln \left[(x-\eta)^2 + y^2 \right]^{0.5} d\eta D_1^4 \right] \right\} \end{aligned} \quad (9)$$

The potential function $F_C(I_{CK})$ for the special crack tip elements can be written in the following form:

$$F_C(I_{CK}) = \int_{-a}^a N_{CK}(\eta) \ln \left[(x-\eta)^2 + y^2 \right]^{0.5} d\eta, \quad \mathbf{K=1 to 4} \quad (10)$$

where I_{C1} to I_{C4} are the integrals for the special crack tip elements distributed from $-a$ to $+a$. These integrals have also been explained in details in [33, 35]. It should be noted that for this case, also two degrees of freedom are used for each node (boundary collocation points) at the center of each sub-element. Based on the linear elastic fracture mechanics (LEFM) principles, the mode I and mode II stress intensity factors K_I and K_{II} can be easily deduced [29, 35]. A crack tip element of length $2a$ is considered, and then the stress intensity factors with respect to the normal and shear displacement discontinuities (assuming plane strain condition) can be determined [32], as:

$$K_I = \frac{\mu}{4(1-\nu)} \left(\frac{2\pi}{a}\right)^{\frac{1}{2}} D_y(a), \quad \text{and} \quad K_{II} = \frac{\mu}{4(1-\nu)} \left(\frac{2\pi}{a}\right)^{\frac{1}{2}} D_x(a) \quad (11)$$

where μ is the shear modulus, and ν is the Poisson ratio of the brittle material.

4. Verification of HODDM

The well-known problem of a central slant crack (see Figure 2) with the existing analytical solution for mode I and II SIFs (stress intensity factors) was chosen to verify the accuracy and applicability of HODDM used. Furthermore, the crack propagation prediction of HODDM was tested against the experimental data. The element length was kept constant (equal to 1 cm) for all the numerical analyses, unless stated otherwise.

4.1. A central slant crack problem

A central slant crack under far field uniform tension is shown in Figure 2. The slant angle $\beta = 45^\circ$ and half crack length $b=1$ m were assumed in the analysis. A crack tip element length to half crack length ratio $l/b = 0.1$ was used for the numerical solution of the problem. The analytical solutions of the first and second mode SIFs, K_I and K_{II} , for the center slant crack problem were given as [28, 37]:

$$K_I = \sigma \sqrt{\pi b \sin^2 \beta} \quad \text{and} \quad K_{II} = \sigma \sqrt{\pi b \sin \beta \cos \beta} \quad (12)$$

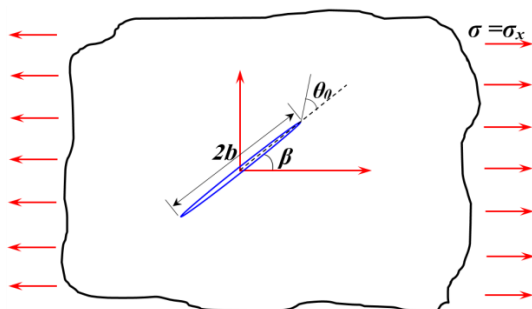


Figure 2. Geometry of a central slant crack problem in an infinite body.

Figure 3 shows the effect of the number of crack tip elements on the SIF prediction in a slant crack problem with $\beta = 45^\circ$. The vertical axis shows the normalized stress intensity factors, while the horizontal axis shows the number of used crack tip elements. The results shown in Figure 3 show that using more crack tip elements increased the accuracy of the method. The most accurate results occurred when four crack tip elements were used. Less than 0.2% error was observed in the prediction of SIFs. Also it should be noted that, based on the analytical solution for the slant crack problem (Eq. (12)), both K_I and K_{II} must be equal for $\beta = 45^\circ$, which is what happened for the numerical results here.

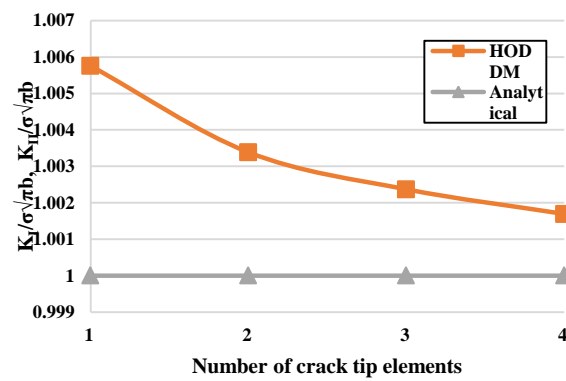


Figure 3. Normalized mode I and II SIFs using HODDM with various numbers of crack tip elements in a 45° slant crack problem.

4.2. Verification of crack propagation prediction by laboratory results

The results obtained for the crack propagation of pre-cracked rock-like cylindrical specimens [33, 38] of 60 mm diameter and 120 mm length were used to verify the capability of HODDM. The mechanical properties of the uncracked rock-like specimens were obtained using the laboratory tests following the ISRM standards. The mechanical properties used in the present analysis were compressive strength, $\sigma_c=28$ MPa; Young's modulus, $E = 15$ GPa, Brazilian tensile strength, $\sigma_t = 3.81$ MPa; and Poisson's ratio, $\nu= 0.21$.

Figure 4 illustrates the geometry and loading conditions of a pre-cracked specimen with three cracks. Cracks 1 and 2 (Isopath cracks) have constant orientations of $\alpha = 60^\circ$. The third crack is oriented at different angles with respect to the direction of cracks 1 and 2, i.e. at the angles $\beta = 0^\circ, 45^\circ, \text{ and } 90^\circ$ (in a counterclockwise direction) (see Figure 4).

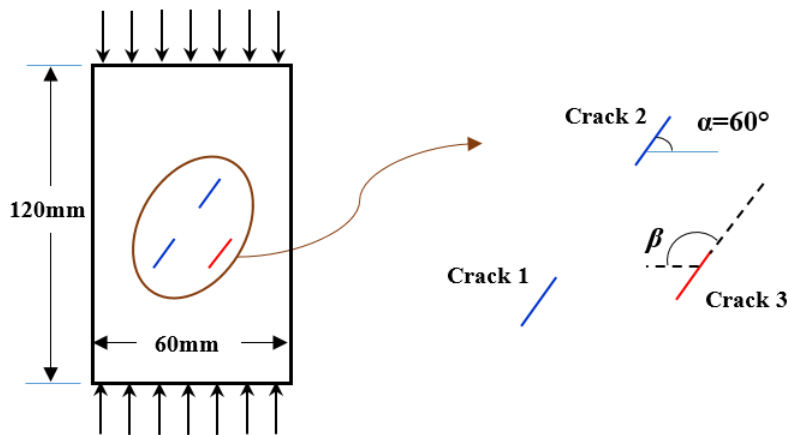


Figure 4. Geometry of two cracks in a pre-cracked rock-like specimen under uniaxial compression.

Figure 5 shows the numerical and experimental results for the crack propagation of the specimens. The numerical results in Figure 6 (a) successfully captured the behavior of the experimental specimens in Figure 6 (b), showing the accuracy and applicability of *HODDM* used. The effects of crack geometry on HF propagation

were then investigated. Two distinct cases were considered in the numerical analyses of the horizontal oil wells: case 1, when all PFs had the same lengths, and case 2, when PFs had different lengths. Also the perforation angle in the vertical oil wells were studied using the two common perforation angles.

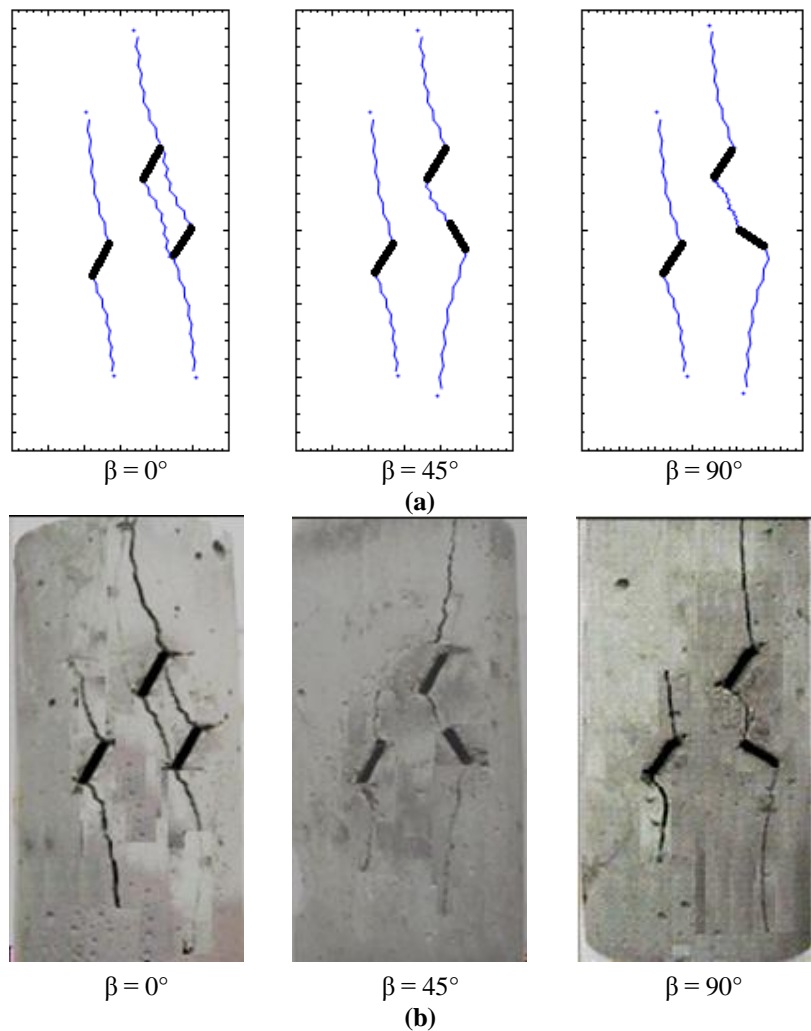


Figure 5. Results of crack propagation paths and crack coalescence for cylindrical specimens (with three cracks) under uniaxial compression: a) numerical b) experimental [33, 38].

5. Analysis of propagation of isolength cracks in HF

Four PFs with equal lengths were modeled on each side of the well. Due to the symmetry of the problem, a line of symmetry was introduced with respect to the boundary elements, as it can be seen in Figure 6. The image elements were used to take into account the effect of symmetrical parts [39]. Figure 7 shows the results obtained for various β s. All models were run for a maximum of 20 steps of crack propagation. For $\beta = 0.125$ and $\beta = 0.5$, inner cracks have not propagated completely, since they were affected by the propagation of the outer cracks and the induced stress field. For $\beta = 0.25$, the inner cracks propagated but the outer cracks were influenced and slowly gained distance from the wellbore and even turned back at the final stages. For the cases of $\beta = 0.75$ and 1.25 , the arrangements were even less productive since

the inner cracks either intersected each other or intersected the outer cracks, which contributed to the near-wellbore tortuosity or even pinching. Both tortuosity and pinching decrease the production rate. When the cracks intersect each other, they produce long and curvy paths through which oil passes to reach the well and finally gets to the surface. These long paths create more friction on the way and reduce the pressure of the reservoir causing a lower production rate. Hence, the intersection of the perforated cracks should be avoided. For $\beta = 1, 1.5,$ and 2 , most crack propagations away from the wellbore happened. Considering that closer cracks achieve a higher permeability, $\beta = 1$ may be reported as the best case for the isolength cracks. This is in close agreement with the results obtained by Yu et al. [40].

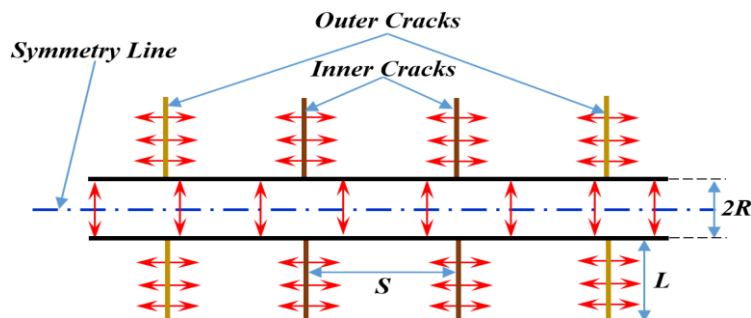


Figure 6. A simple sketch of model with geometrical parameters.

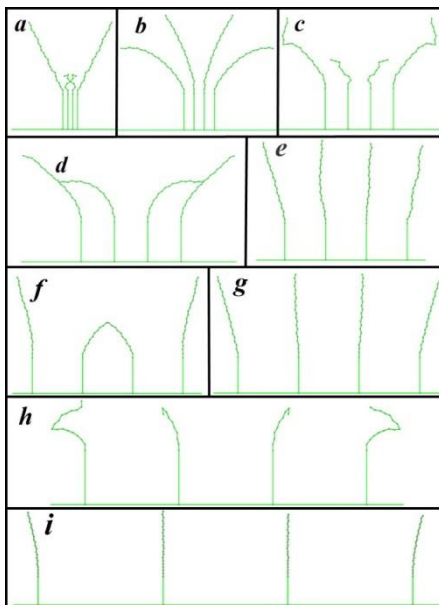


Figure 7. Crack propagation for different fracture spacing factors: a) $\beta = 0.125$, b) $\beta = 0.25$, c) $\beta = 0.5$, d) $\beta = 0.75$, e) $\beta = 1.0$, f) $\beta = 1.25$, g) $\beta = 1.5$, h) $\beta = 1.75$, and i) $\beta = 2.0$.

Figure 8 shows the effect of fracture spacing (in foot) on the measured cumulative gas production

(in million standard cubic feet), shown by Yu et al. [40]. The fractures in their study were 250 ft long. As it can be seen in this figure, the production increases with increase in spacing up to almost 250 ft, and then it remains constant for larger spacings, implying an optimum distance equal to the fracture length (250 ft). The sharp slope of the diagram before spacing = 100 ft shows a low production, which is probably caused by interference of the fractures in smaller spacings, which was also observed in the current study.

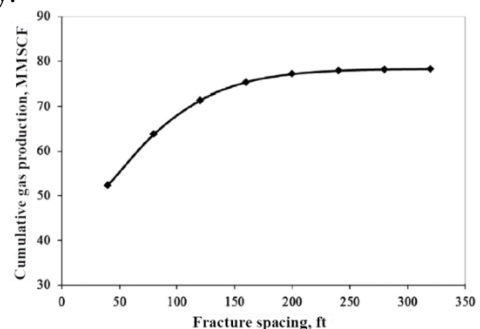


Figure 8. Effect of fracture spacing on cumulative gas production in base well with equal number of fractures [40].

6. Analysis of propagation of cracks with different lengths in HF

The effect of crack length on the crack propagation was investigated using two different lengths L_1 and L_2 ($L_1 > L_2$) for perforated fractures. Two combinations of PFs were studied. In the first combination, two PFs with the length of L_1 were used as the outer cracks, while the inner cracks had an L_2 length. In the second combination, the inner and outer crack lengths were replaced.

It can clearly be seen in the crack propagations in Figure 9 that for the first combination, the near-wellbore tortuosity was more frequently happening than the isolength cracks. For $\beta = 0.125, 0.25, 0.75,$ and 1.25 , the inner cracks intersected the outer cracks or intersected each other. For $\beta = 0.5$ and 1 , the intersection of cracks were also possible in more analytic steps.

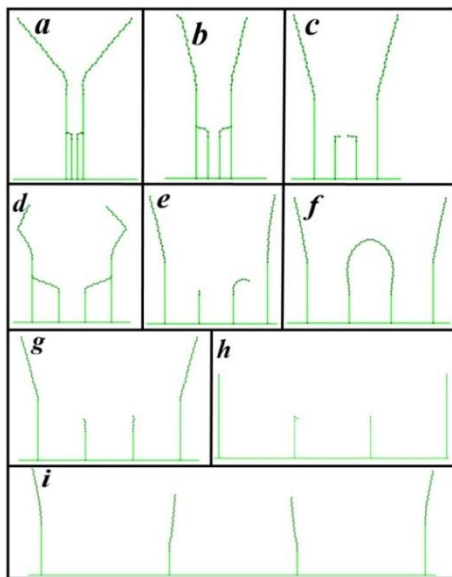


Figure 9. Hydraulic fracture propagations for first combination (longer outer cracks): a) $\beta = 0.125$, b) $\beta = 0.25$, c) $\beta = 0.5$, d) $\beta = 0.75$, e) $\beta = 1.0$, f) $\beta = 1.25$, g) $\beta = 1.5$, h) $\beta = 1.75$, and i) $\beta = 2.0$.

In the second combination for $\beta = 0.125, 0.25, 0.75,$ and 1.0 , the outer cracks interfered with the inner cracks (Figure 10). For $\beta = 0.5$ and 1.0 , the

outer cracks could not propagate much, and were arrested at the first steps. The cracks were almost fully propagated for $\beta = 1.25, 1.5,$ and 2.0 , while for $\beta = 1.75$, the cracks could not propagate much away from the wellbore. Following the same reasoning, the best case may be $\beta = 1.25$ for a better permeability achievement.

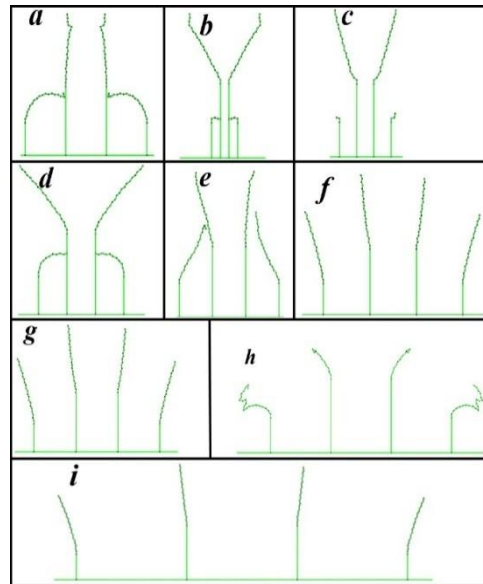


Figure 10. Hydraulic fracture propagations for second combination (longer inner cracks): a) $\beta = 0.125$, b) $\beta = 0.25$, c) $\beta = 0.5$, d) $\beta = 0.75$, e) $\beta = 1.0$, f) $\beta = 1.25$, g) $\beta = 1.5$, h) $\beta = 1.75$, and i) $\beta = 2.0$.

7. Propagation of cracks perforated with a phase angle

Perforation of wellbore may be carried out with a phase angle. A vertical well of the same geometry was considered to study the perforation angle in this section. Two commonly used phases of $\phi = 60^\circ$ and 120° were studied. The cracks were rotated in relation to σ_H , i.e. x-axis. Figure 11 shows the sketch of the primary models. For $\phi = 60^\circ$, the inclination angle $\beta = 0^\circ, 15^\circ, 30^\circ,$ and 45° , and for the $\phi = 120^\circ$ angle, $\beta = 0^\circ, 15^\circ, 30^\circ, 45^\circ, 60^\circ, 90^\circ,$ and 105° were considered.

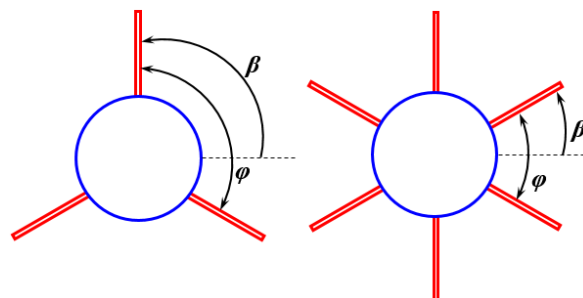


Figure 11. PFs with a phase angle ϕ and starting angle β .

Figure 12 shows the crack propagations for variations in $\varphi = 60^\circ$. In Figure 12(a), only those cracks aligned with σ_H propagated. The cracks orienting more than 45° showed no tendency to propagate. The best results were obtained for $\beta = 30^\circ$, where the two sets of cracks were oriented 30° from σ_H . As it can be seen, one set of cracks being perpendicular to σ_H did not propagate in Figure 12 (c) but the other two sets fully propagated. As expected for $\beta = 15^\circ$ and 45° in

Figures 12 (b) and (d), the least propagation occurred since in these two sets of cracks, $\beta > 45^\circ$. Figure 13 shows the crack propagations for variations in $\varphi = 120^\circ$. The cracks perpendicular to σ_H did not propagate (Figures 13 (c) and (g)), while for the other inclination angles, the cracks fully propagated. A comparison of the results using Figures 12 and 13 showed that the cracks with the phase angle $\varphi = 120^\circ$ resulted in a better crack propagation in the HF procedure.

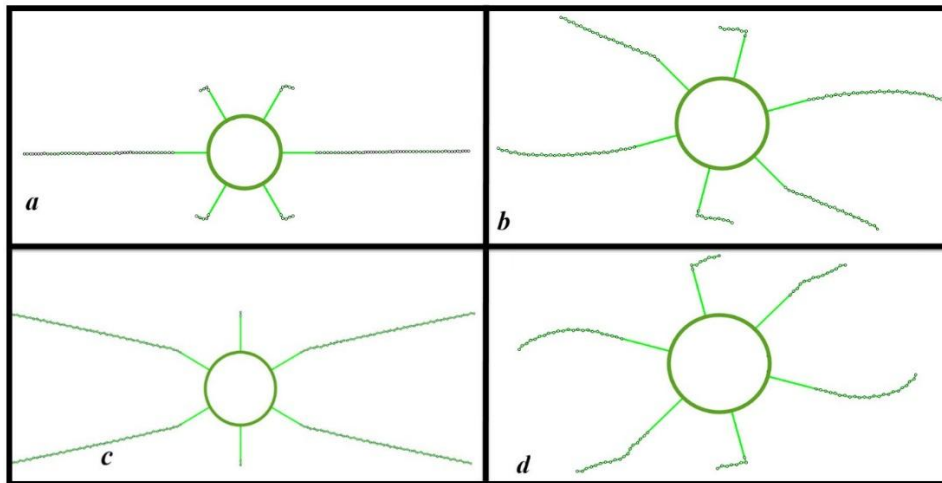


Figure 12. Variations in crack propagations of PFs with phase angle $\varphi = 60^\circ$: a) $\beta = 0^\circ$, b) $\beta = 15^\circ$, c) $\beta = 30^\circ$, and d) $\beta = 45^\circ$.

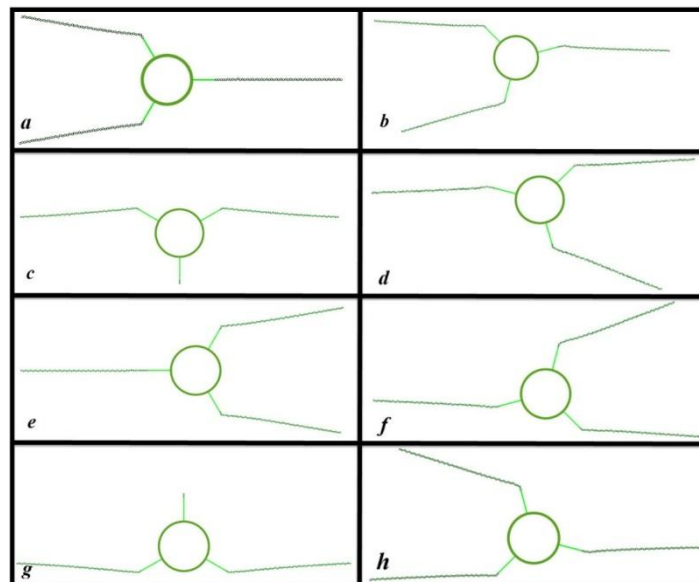


Figure 13. Variations in crack propagations of PFs with phase angle $\varphi = 120^\circ$: a) $\beta = 0^\circ$, b) $\beta = 15^\circ$, c) $\beta = 30^\circ$, d) $\beta = 45^\circ$, e) $\beta = 60^\circ$, f) $\beta = 75^\circ$, g) $\beta = 90^\circ$, and h) $\beta = 105^\circ$.

8. Conclusions

The geometrical parameters involved in the hydraulic fracturing (HF) in a horizontal wellbore were studied using a 2D *HODDM* code. Different crack lengths and spacings were used in the model to investigate the interaction of cracks with their

propagation. A maximum of 20 steps of crack propagation was considered for each case. A fracture spacing factor was used to generalize the results. For the isolength cracks, the best results were obtained for $\beta = 1.0, 1.5,$ and 2 . Since closer

cracks contributed to higher permeabilities, $\beta = 1$ may be introduced as the best case for HF, i.e. the spacings and crack lengths should be equal. This was in close agreement with the results obtained from the other studies. When the outer cracks were longer, the best case was for $\beta = 2.0$, while when the inner cracks were longer, the best case was for $\beta = 1.25$. Based on the numerical results obtained, the best crack propagation occurred when all PFs were of the same size, and the worst case was for the longer outer cracks, where there was no significant crack propagation for close spacings.

Two common perforation phases for HF in the vertical wells were also studied, which resulted in the following conclusions. For the phase angle $\varphi = 60^\circ$, best results were obtained for $\beta = 30^\circ$, and more deviation from σ_H did not produce better results similar to those obtained for the single and double sets of PFs. For the phase angle $\varphi = 120^\circ$, all PFs fully propagated, except for those perpendicular to σ_H . The best results may be obtained using $\varphi = 120^\circ$, with any deviation from σ_H , except for $\beta = 30^\circ$ and 90° .

References

- [1]. Rahman, M., Hossain, M. and Rahman, S. (2000). Hydraulic fracture initiation and propagation: roles of wellbore trajectory, perforation and stress regimes. *J Pet Sci Eng.* 27: 129-149.
- [2]. Chitrala, Y., Moreno, C., Sondergeld, C. and Rai, C. (2013). An experimental investigation into hydraulic fracture propagation under different applied stresses in tight sands using acoustic emissions. *J Pet Sci Eng.* 108:151-161.
- [3]. Freeman, C.M., Moridis, G., Ilk, D. and Blasingame, T.A. (2013). A numerical study of performance for tight gas and shale gas reservoir systems. *J Pet Sci Eng.* 108: 22-39.
- [4]. Baujard, C. and Bruel, D. (2006). Numerical study of the impact of fluid density on the pressure distribution and stimulated volume in the Soultz HDR reservoir. *Geothermics.* 35: 607-621.
- [5]. Zhao, Y-L., Zhang, L-H., Luo, J-X. and Zhang, B-N. (2014). Performance of fractured horizontal well with stimulated reservoir volume in unconventional gas reservoir. *J Hydrol.* 512: 447-456.
- [6]. Guo, T., Zhang, S., Qu, Z., Zhou, T., Xiao, Y. and Gao, J. (2014). Experimental study of hydraulic fracturing for shale by stimulated reservoir volume. *Fuel.* 128: 373-380.
- [7]. Ajao, O., Iwu, C.F., Dalamarinis, P. and Economides, M.J. (2013). Case studies for the fracturing of highly diverse gas reservoirs. *J Nat Gas Sci Eng.* 14: 34-41.
- [8]. Davies, R., Foulger, G., Bindley, A. and Styles, P. (2013). Induced seismicity and hydraulic fracturing for the recovery of hydrocarbons. *Mar Pet Geol.* 45: 171-185.
- [9]. Kaiser, M.J. (2012). Haynesville shale play economic analysis. *J Pet Sci Eng.* 82-83: 75-89.
- [10]. Kalantari-Dahaghi, A. (2011). Systematic approach to numerical simulation and modeling of shale gas reservoirs. *Int J Oil Gas Coal Technol.* 4: 209-243.
- [11]. Fazelpour, W. (2011). Development of techniques to integrate hydraulic fracturing design and reservoir simulation technologies- application to forecast production of stimulated wells in unconventional gas reservoirs. *SPE Middle East Unconv. Gas Conf. Exhib., Muscat, Oman.*
- [12]. Castaneda, J.C., Castro, L., Craig, S., Moore, C. and Myatt, J. (2010). Coiled tubing fracturing: an operational review of a 43-stage Barnett shale stimulation. *SPE/ICoTA Coiled Tubing Well Interv., The Woodlands.*
- [13]. King, G.E. (2010). Thirty years of gas shale fracturing: what have we learned. *SPE Annu. Tech. Conf. Exhib., Florence, Italy.*
- [14]. Jaeger, J., Cook, N. and Zimmerman, R. (2009). *Fundamentals of rock mechanics.*
- [15]. Brudy, M. and Zoback, M.D. (1999). Drilling-induced tensile wall-fractures: implications for determination of in-situ stress orientation and magnitude. *Int J Rock Mech Min Sci.* 36: 191-215.
- [16]. Nelson, E.J., Meyer, J.J., Hillis, R.R. and Mildren, S.D. (2005). Transverse drilling induced tensile fractures in the West Tuna area, Gippsland Basin, Australia: implications for the in situ stress regime, *Int J Rock Mech Min Sci.* 42: 361-371.
- [17]. Zhou, J., Chen, M., Jin, Y. and Zhang, G. (2008). Analysis of fracture propagation behavior and fracture geometry using a tri-axial fracturing system in naturally fractured reservoirs. *Int J Rock Mech Min Sci.* 45: 1143-1152.
- [18]. Cherny, S., Chirkov, D., Lapin, V., Muranov, A., Bannikov, D., Miller, M., Willberg, D., Medvedev, O. and Alekseenko, O. (2009). Two-dimensional modeling of the near-wellbore fracture tortuosity effect. *Int J Rock Mech Min Sci.* 46: 992-1000.
- [19]. Linkov, A.M. (2012). On efficient simulation of hydraulic fracturing in terms of particle velocity. *Int J Eng Sci.* 52: 77-88.
- [20]. Zhang, G.Q. and Chen, M. (2010). Dynamic fracture propagation in hydraulic re-fracturing. *J Pet Sci Eng.* 70: 266-272.
- [21]. Huang, J., Griffiths, D. and Wong, S.W. (2012). Initiation pressure, location and orientation of hydraulic fracture. *Int J Rock Mech Min Sci.* 49: 59-

67.

- [22]. Guangqing, Z. and Mian, C. (2009). Complex fracture shapes in hydraulic fracturing with orientated perforations. *Pet Explor Dev.* 36: 103-107.
- [23]. Xu, Y., Zhai, C., Hao, L., Sun, X., Liu, Y., Li, X. and Li, Q. (2011). The Pressure Relief and Permeability Increase Mechanism of Crossing-Layers Directional Hydraulic Fracturing and Its Application. *Procedia Eng* 2011. 26: 1184-1193.
- [24]. Mohammadnejad, T. and Khoei, R. (2013). An extended finite element method for hydraulic fracture propagation in deformable porous media with the cohesive crack model. *Finite Elem Anal Des.* 73: 77-95.
- [25]. Chen, Z., Bungler, A., Zhang, X. and Jeffrey, R. (2009). Cohesive zone finite element-based modeling of hydraulic fractures. *Acta Mech Solida Sin.* 22: 443-52.
- [26]. Rahman, M.M., Hossain, M.M., Crosby, D.G. and Rahman, M.K. (2002). Analytical, numerical and experimental investigations of transverse fracture propagation from horizontal wells. *J Pet Sci Eng.* 35: 127-50.
- [27]. Erdogan, F. and Sih, G.C. (1963). On the crack extension in plates under plate loading and transverse shear. *J Basic Eng.* 85: 519-27.
- [28]. Whittaker, B.N., Singh, R.N. and Sun, G. (1992). *Rock fracture mechanics, principles design and applications.* Netherland.
- [29]. Sanford, R.J. (2003). *Principles of fracture mechanics.* USA: Prentice Hall.
- [30]. Fatehi Marji, M. (2014). *Rock fracture mechanics with displacement discontinuity method.* Germany: LAP Lambert Academic publishing.
- [31]. Fatehi Marji, M. (2015). Higher order displacement discontinuity method in rock fracture mechanics. Yazd University.
- [32]. Shou, K.J. and Crouch, S.L. (1995). A higher order displacement discontinuity method for analysis of crack problems. *Int J Rock Mech Min Sci Geomech Abstr.* 32: 49-55.
- [33]. Abdollahipour, A., Fatehi Marji, M., Yarahmadi-Bafghi, A. and Gholamnejad, J. (2015). Simulating the propagation of hydraulic fractures from a circular wellbore using the Displacement Discontinuity Method. *Int J Rock Mech Min Sci.* 80: 281-291.
- [34]. Fatehi Marji, M., Hosseini-Nasab, H. and Morshedi, A.H. (2009). Numerical modeling of the mechanism of crack propagation in rocks under TBM disc cutters. *Mech Mater Struct.* 4: 605-627.
- [35]. Fatehi Marji, M., Hosseini Nasab, H. and Kohsary, A.H. (2006). On the uses of special crack tip elements in numerical rock fracture mechanics. *Int J Solids Struct.* 43: 1669-1692.
- [36]. Crouch, S.L. (1976). Solution of plane elasticity problems by the displacement discontinuity method. I. Infinite body solution. *Int J Numer Methods Eng.* 10: 301-343.
- [37]. Guo, H., Aziz, N.I. and Schmitt, L.C. (1990). Linear elastic crack tip modeling by displacement discontinuity method. *Engin Fract Mech.* 36: 933-943.
- [38]. Haeri, H., Shahriar, K., Fatehi Marji, M. and Moarefvand, P. (2014). On the cracks coalescence mechanism and cracks propagation paths in rock-like specimens containing pre-existing random cracks under compression. *J Cent South Univ.* 2404-2414
- [39]. Crouch, S.L. and Starfield, A.M. (1983). *Boundary Element Methods in Solid Mechanics.* London: George allen & Unwin.
- [40]. Yu, W., Luo, Z., Javadpour, F., Varavei, A. and Sepehrnoori, K. (2014). Sensitivity analysis of hydraulic fracture geometry in shale gas reservoirs. *J Pet Sci Eng.* 113: 1-7.

بررسی عددی تأثیر پارامترهای هندسی ترک بر فرآیند شکست هیدرولیکی در مخازن هیدروکربنی

ابوالفضل عبداللهی پور*، محمد فاتحی مرجی، علیرضا یاراحمدی بافقی و جواد غلام نژاد

دانشکده مهندسی معدن و متالورژی، دانشگاه یزد، ایران

ارسال ۲۰۱۵/۱۰/۰۷، پذیرش ۲۰۱۵/۱۱/۲۴

* نویسنده مسئول مکاتبات: ab.abdollahipour@gmail.com

چکیده:

شکست هیدرولیکی، به‌عنوان یک روش تحریک در مهندسی نفت، تولید نفت از مخازن با نفوذپذیری بسیار کم را ممکن کرده است. ترکیب حفاری افقی و شکست هیدرولیکی چندگانه با زوایای گوناگون مشبک‌کاری برای تحریک مخازن و تولید اقتصادی به‌صورت متداول به کار می‌رود. برخلاف استفاده رایج از شکست هیدرولیکی همچنان جنبه‌های گوناگونی از این عملیات مبهم است و نیاز به تحقیق و بررسی بیشتر دارد؛ بنابراین، بهینه‌سازی هندسه شکستگی‌های اولیه با استفاده از روش‌های عددی اهمیت بالایی در موفقیت‌آمیز بودن عملیات شکست هیدرولیکی دارد. پارامترهای هندسی متفاوت در ترک‌های اولیه شکست هیدرولیکی شامل الگو، فاصله‌داری، طول ترک و زاویه فازی مشبک‌کاری با استفاده از روش ناپیوستگی جابجایی مرتبه بالاتر در چاه‌های افقی و قائم مدلسازی شدند. چندین مسئله شناخته‌شده در شکست هیدرولیکی مانند تداخل ترک و توقف ترک در الگوهای خاص قرارگیری ترک‌های اولیه مشاهده شد. نتایج حاصل با اندازه‌گیری‌های برجا موجود در مطالعات گذشته تائید شد. علاوه بر این، بهترین زاویه مشبک‌کاری در چاه‌های قائم بررسی و تعیین شد.

کلمات کلیدی: شکست هیدرولیکی، شبیه‌سازی چاه، گسترش ترک، تداخل ترک، مشبک‌کاری.
